A study on Segmentation of Retinal Layers in OCT images for disease analysis

H Pallab Jyoti Dutta[1], Dr. S. R. Nirmala[*1]
[1]*Department of ECE,*
Gauhati University Institute of Science and Technology, Gauhati University,
(E-mail: [1]pallabhp@gmail.com, [*]nirmalasr3@gmail.com)

***Abstract*—** Optical Coherence Tomography (OCT) is a non-invasive imaging technique that proved to be a quintessential image capturing device from within the biological tissues. It helps greatly in monitoring the characteristics and morphology of retinal layers. This paper gives an insight about different research works done with the aim of automatically segmenting the different layers of retina in an OCT retinal image using different groundbreaking techniques such as graph theory and dynamic programming, SVM, diffusion process, active contours etc. This automatic segmentation will help in addressing the problem of time consuming, labor oriented and personnel dependent manual segmentation process and also help in proper and accurate diagnosis of disease related to eyes. Though the segmentation of normal retina is done with some accuracy, segmentation of retina with pathology is still a challenge. It also throws light on Retinopathy of Prematurity, which is an eye disease affecting the eyes of the prematurely born babies and one of the primary reasons for childhood blindness. Its development and affects can be observed proficiently through an OCT system and segmentation of the retinal layers goes the extra mile as far as helping with the proper diagnosis of the pathology is concerned.

***Keywords*—** *Image Segmentation, Optical Coherence Tomography, Retinal Layers, Retinopathy of Prematurity.*

I. INTRODUCTION

Segmentation of retinal layers in an OCT image is primarily required to analyze the different layers of retina in a detailed manner and with the availability of the technology, the doctors and the researchers encourage the work on segmenting the layers for the diagnosis and further procurement of available information embedded in the image respectively.

Image segmentation is the process of partitioning a digital image into segments, containing each pixel with similar characteristics, so as to simplify and represent the image in a meaningful and easier way to analyse. Image segmentation is used to detect objects and boundaries (lines, curves, etc.) in images. Precisely speaking, image segmentation is the process where every pixel in an image is assigned a label, such that the pixels with the same label contain certain characteristics [1]. Meaningful segmentation is the first step in converting low-level image processing into high-level image description in terms of features, objects, and scenes.

Now this segmentation of the OCT image furnishes the requisite information related to the morphology of the retina. Optical Coherence Tomography (OCT) is a medical non-invasive imaging technique that uses light to capture micrometer resolution, 3-D images from within optically scattering media e.g. biological tissues [2]. In simple terms, Optical Coherence Tomography, if we see the meaning of each word, Optical refers to light, Coherence means that the light is of constant phase difference which is analogous to monochromatic light and Tomography refers to imaging by slices. So, when put together it is defined as the image of the tissue viewed through the slices using the coherent property of light. It is based on low coherence inferometry [2] employing near infrared light. The use of relatively long wavelength light allows it to penetrate into the scattering media.

Light in an OCT system is divided into 2 arms- an arm containing the item of interest and a reference arm usually containing a mirror [2]. The combination of reflected light from the arm of interest and the reference arm gives rise to an interference pattern but only if the light from both the arms have travelled the same distance. By scanning the mirror in the reference arm, a reflectivity profile of the sample can be obtained, which is called an A-scan, which again contains information about the spatial dimensions and location of the structures within the item of interest. A cross-sectional tomography, called B-scan, may be formed by combining a series of these A-scans laterally.

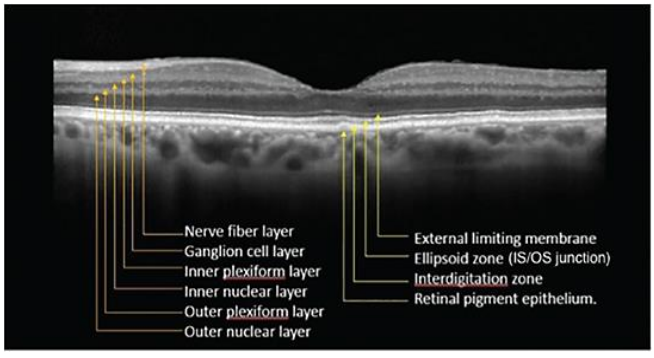

Fig. 1. Different layers of retina [2].

An image of OCT retinal image showing its different layers [2] is shown in Fig. 1. Briefly, the layers are [3]:

- The retinal nerve fiber layer is formed due to expansion of optic nerve fibers.
- The ganglion cell layer constitutes ganglion cells and displaced amacrine cells.
- The inner plexiform layer is formed by a dense reticulum of fibrils which is a result of interlaced cells of the inner nuclear layer and dendrites of ganglion cells.
- The inner nuclear layer is formed by bipolar cells, horizontal cells, and amacrine cells.
- The outer plexiform layer is made up of synapses between photoreceptor cell from the outer nuclear layer and dendrites of horizontal cells from the inner nuclear layer.
- The outer nuclear layer contains several strata of rod and cone granules.
- External Limiting Membrane is the intercellular junction between photoreceptor cells and between photoreceptor and Muller cells.
- The photoreceptor layers consist of the segments of rods and cones in retina.
- Retinal pigment epithelium (RPE) is the pigmented cell layer above the choroid of the eye and just outside the neurosensory retina that nourishes retinal visual cells.

An OCT image provides a lot of information about the retinal layers such as the thickness, presence of any drusen or other substance, retinal detachment, lesions that cannot be detected in other kinds of images of the retina, any kind of elevation or depression of the retinal layers which prove to be proficient in detection of different kinds of pathologies.

The remaining part of this paper is systematized in the following way: Section II documents the previous literary works or the different methodologies in segmentation of retinal OCT images and also gives an idea about the observations of a few medical papers and a brief description of ROP, one of the primary causes of childhood blindness. Section III concludes the paper.

II. RESEARCH WORKS

Different researchers took into account the information present in the OCT image, pertaining to the retinal layers, analyzed it and proposed pioneering techniques to segment the layers. In the recent times, with the improvement of image processing techniques, researchers have turned their attention towards automatic segmentation of the retinal layers, and reduce the use of time consuming and labor oriented manual segmentation methods. The first five papers deal with normal eyes whereas the remaining papers address the retina affected by pathologies.

Fernández et al. (2005) [5] employs an enhancement segmentation approach for noise reduction and segmentation. Here a non-linear complex diffusion process [23] is used for denoising and edge detection, followed by a coherence enhanced diffusion filter [22] to improve discontinuities of the layers and obtain structure coherence matrix. The non-linear complex diffusion process uses the complex domain diffusion coefficients for a robust edge detection through smoothed second derivative of the initial signal scaled by time. The equation for the nonlinear complex diffusion approach is:

$$\frac{\partial}{\partial t} I = \nabla.(d(Im(I))\nabla I) \quad (1)$$

where Im(.) is the imaginary value and the diffusivity is defined as:

$$d(Im(I)) = (exp(i\theta))/(1 + (Im(I)/k\theta)^2) \quad (2)$$

where k is a threshold parameter and $\theta\epsilon(-\pi/2;\pi/2)$ is the phase angle. In the coherence enhanced diffusion filtering the diffusion process is guided by a diffusion tensor which varies for both edge location and orient- ation, thus facilitating a true anisotropic diffusion process (i.e. a process of removing the noise without affecting the edge information). It is governed by the following equation:

$$\frac{\partial}{\partial t} I = \nabla.(\boldsymbol{d}(I)\nabla I) \quad (3)$$

where the diffusion tensor d is chosen to enhance coherence. Using the automatic peak finding procedure (which uses the coherence matrix) and detecting the max intensity level, different layers are detected. The peaks of different layers are shown in Fig. 2. The boundaries are approximated using linear interpolation to correct discontinuous segments. Here a total of 7 edges are extracted from 72 OCT scans of normal subjects. Its result is shown in Fig. 3. However this algorithm does not provide satisfactory result in case of pathologies.

Rossant et al. (2009) [6], the authors put forwarded a method of segmenting 8 retinal layers. Their main aim was to deduce a method that is quite immune to noise, reduce the use of training set and parameters and seg- ment the layers around fovea. Hence they emphasized on developing a method based on global segmentation algorithm. First they preprocessed the image using a non-linear diffusion filter [18], followed by detecting the Inner Limiting Membrane (ILM) by an edge-tracking algorithm and regularized it by an active contour [19] algorithm. Then they detected the fovea and Hyper Reflective Complex (HRC) which comprises of ChCap (Choriocapillaries), Retinal Pig- ment Epithelium (RPE) and Outer Segment (OS) layers by iteratively deducing a median line that allows approximating its distance from HRC edges and initializing an active contour. The photoreceptor IS-OS layer is extracted using a peak detector and a kalman filter is employed to detect the ONL/IS and OS/RPE edges. The Kalman filter is defined by a state vector X that characterizes the tracked pixels, and a theoretical model that allows predicting the evolution of X. In their application, the state

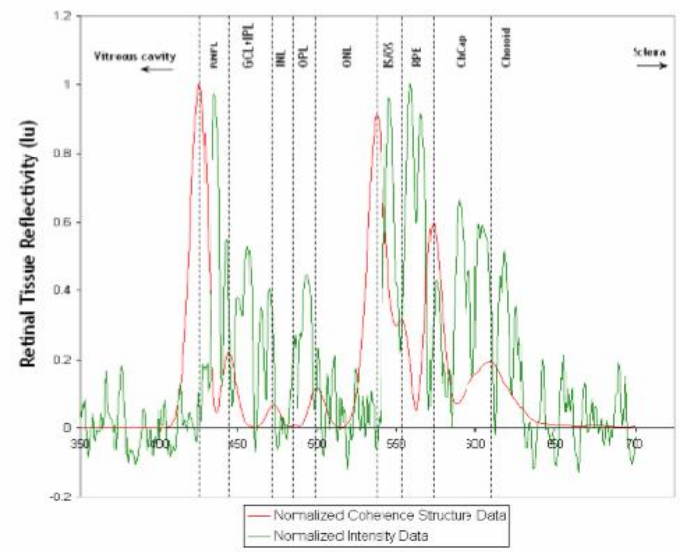

Fig. 2. Segmentation of an A-scan line based on the coherence structure information extracted from the OCT signal intensity after enhancing diffusion filtering. [5].

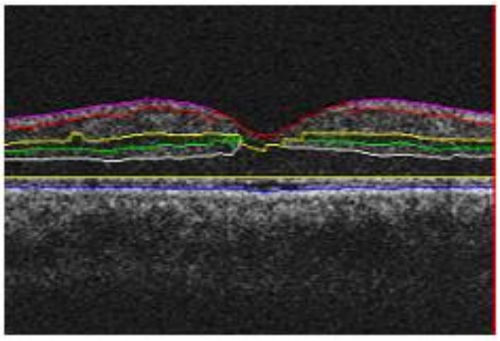

Fig. 3. Automatic segmentation result [5].

vector includes the intensity value of the pixel and its distance to the IS/OS line. Finally the inner layers comprising RNFL (Retinal Nerve Fiber Layer), OPL/ONL (Outer Plexiform Layer/Outer Nuclear Layer) edges, GCL+IPL/INL (Ganglion Cell Layer + Inner Plexiform Layer/Inner Nuclear Layer) edges, INL/OPL edges are segmented using k-means and Markov Random field [20] techniques. They implemented the method on 72 images from normal subjects and compared the results with those obtained by 5 experts which show good accuracy and correlation between the results. Also the distance between the manually segmented interfaces and the automated ones show the accuracy of the proposed method. However the performance of the method in presence of pathologies is unknown.

Lee et al. (2013) [7] segments 3 layers (ILM, RPE and Bruch's Membrane) using automatic segmentation software DOCTRAP and also compares the thickness measurement results obtained with the respective semiautomatic segmentation software of the Spectralis and Cirrus. Here they employ flattening the image based on a pilot estimate of Bruch's Membrane, by fitting to a polynomial and calculate the graph weights using gradient, intensity and distance information. Then they use the shortest path algorithm to segment the layers. A total of 40 SD-OCT scans from 20 subjects for each machine were included where the mean thickness in the 1-mm central area determined by DOCTRAP and Spectralis was 463.8 ± 107.5 µm and 467.0 ± 108.1 µm, respectively and the mean thickness in the 1-mm central area was 440.8 ± 183.4 µm and 442.7 ± 182.4 µm by DOCTRAP and Cirrus, respectively. The segmentation result is shown in Fig. 4.

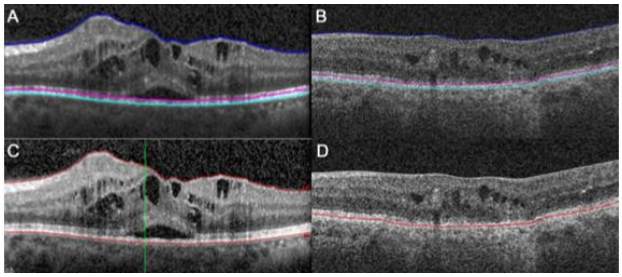

Fig. 4. Automatic segmentation results. (A, B) DOCTRAP segmentation of a (C) Spectralis and a (D) Cirrus image. [7].

Duan et al.(2015) [8] proposes a method of segmenting retinal layers using a variational retinex model [25], which take into account reflectance and illumination of the image to pose the retinex problem, to enhance the details and correct inhomogeneities. They used a variational functional for image enhancement which is minimized. The variational function is given by:

$$E(r) = \alpha \int_{\Omega} r^2 + \int_{\Omega} |\nabla(s-r)|^2 + \beta \int_{\Omega} |\nabla r| \qquad (4)$$

with constraint r ≤ 0. In the equation r is reflectance, l is illumination and s=r+l. α and β are coefficients. An anisotropic coherent enhancing diffusion [29] is used to remove speckle noise and connect interrupted boundaries. It is governed by:

$$\partial_t u = div(\mathbf{D}(\mathbf{J}_p)\nabla u) \qquad (5)$$

where **J**p is the smoothed version of the structure tensor **J** by using a Gaussian kernel with standard deviation p. Here the segmentation process is done in two stages where, in the first stage an isotropic filter [27] removes the low contrast edges and obtains the thick layers by using a region growing method. The isotropic diffusion is proposed as:

$$\partial_t u = div(g(|\nabla u_\sigma|)\nabla u) \qquad (6)$$

where $g(|\nabla u_\sigma|)$ is a non-increasing diffusivity. In the second stage, an unsharp masking filter sharpens the thin or low contrast layers and applies the region growing algorithm. The definition of unsharp masking is:

$$g = f + k(f - G_\sigma * f) \qquad (7)$$

where f is blurred input image, an k is a positive parameter. G_σ is Gaussian kernel with standard deviation σ. Thus, the layers

are segmented accordingly as shown in Fig. 5.

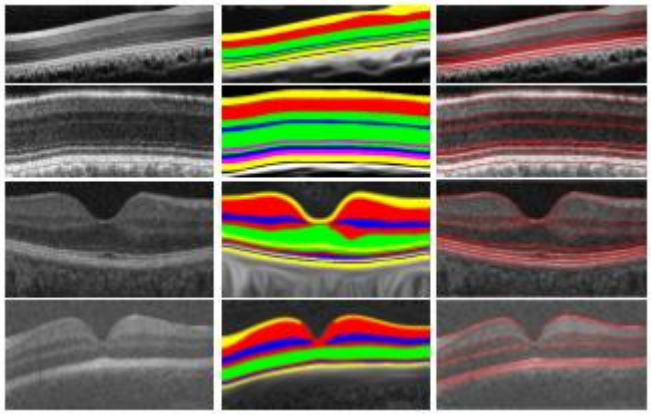

Fig. 5. Segmentation results. 1st column: Original images; 2nd column: Combined the two segmentation results with different colors drawn on different retinal layers; 3rd column: Final results shown in reds [8].

Gao et al. (2016) [9] segments 10 layers of OCT retinal image by using Graph Optimal Approach. Instead of considering the intensity or gradient features of the single-pixel, the proposed method focuses on the whole edge-based image cues. They constructed a weighted graph to acquire the gradient information and spatial relationship. The weight matrix is given by:

$$W(i,j)=f(W_R(i,j))*W_G(i,j) \quad (8)$$

$$f(W_R(i,j))=-(W_R(i,j)-R_0)*(W_R(i,j)-R_1) \quad (9)$$

where, $W_G(i,j) = \exp(g_i + g_j)$ and $W_R(i,j) = ||r_i - r_j||$. The g_i and g_j denote the sum of the connected components corresponding to two nodes in the gradient of the pixels. The r_i and r_j denote the mean of the connected components corresponding to two nodes in the row- coordinate of the pixels, and the parameter R_0 and R_1 control the feasibility distance between true boundaries.

Then they detected the two high contrast boundaries (ILM-IS/CL(Connecting Cilia)) by constructing a graph using high contrast connected components detected by a canny edge detector. Similarly, just by changing the threshold value of the detector 4 low or middle contrast boundaries (ELM (External Limiting Membrane) and below ELM) and five low or middle contrast boundaries above ELM are detected. The result is shown in Fig. 6.

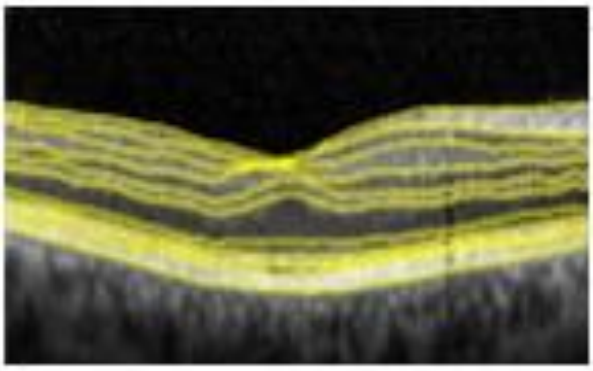

Fig. 6. Final segmentation using graph optimal method [9].

Chiu et al. (2010) [10] This research work is done with the aim of reducing the use of time consuming manual segmentation process of OCT retinal images. This paper segments 7 retinal layers automatically using graph theory and dynamic programming [28]. The authors have addressed the problem of merging of retinal layers at the fovea and uneven tissue reflectivity. Here they first flatten the image based on a pilot estimate of RPE and calculate the graph weights. Weights are calculated as follows:

$$w_{ab}=2-(g_a+g_b)+w_{min} \quad (10)$$

where w_{ab} is the weight assigned to the edge connecting pixels a and b, g_a is the vertical gradient of the image at pixel a, g_b is the vertical gradient of the image at pixel b, w_{min} is the minimum weight of the graph.

An interesting feature of the proposed method is the automatic start and end point selection. Using Dijkstra's method they opted to find the shortest path that accurately cuts the layers. They also derived two adjacency matrices representing the graph weights, which operate differently for dark-to-light or light-to-dark intensity transitions, which is clearly evident among the retinal layers. Through an iterative application of the above mentioned ways, they segmented the high contrast layers first i.e. the vitreous- NFL and IS-OS layer boundaries. Each time they segmented the layers they limited the search region using intensity profiling and connectivity based segmentation. Then they went to detect the vessel location and segmented the NFL- GCL boundary and detected the fovea if present and segment the IPL to ONL layer boundaries and finally the IS to choroid layer boundaries. The result of the method compared with manually segmented scans is shown in Fig. 7. The mean difference (in pixel) in total retinal thickness between two expert manual graders as compared to the thickness differences between the automatic segmentation and one expert manual grader is found out to be 2.22 pixels and 0.92 pixels respectively. This establishes the accuracy of the method. However, this paper mainly concerns normal eye. The retina affected by disease is discussed in the following paper.

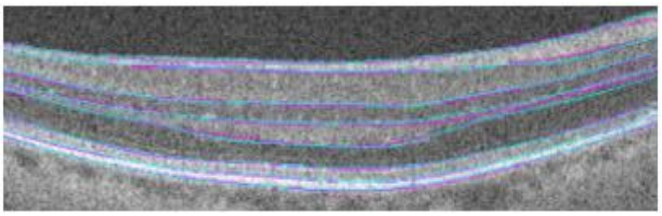

Fig. 7. Comparison of automatic (cyan) versus manual (magenta) segmentation [10].

Chiu et al. (2012) [13] have also presented an automatic segmentation method of retinal OCT images with AMD including Drusen and Geographic Atrophy. Here they segment ILM, RPEDC (Retinal Pigment Epithelium Drusen Complex) and Bruch's Membrane. This paper try to address the accuracy of segmentation for disease affected retina which is hard to achieve. This paper too employs graph theory and dynamic programming [10]. Here they separate the NFL-OPL and IS-RPE boundaries, flattens the image, calculate graph weights, limits the search region and find the shortest path and

iteratively continue the process till the required layers are segmented. For this paper they used a modified form of equation (4), as to delineate the ILM, weights assigned to a dark-to-light adjacency matrix are calculated based on this equation:

$$w_{ab} = \text{normalize}(-(g_a^{DL} + g_b^{DL}),0,1) + w_{min} \quad (11)$$

where, w_{ab} is the edge weight connecting pixels a and b, g_a^{DL} and g_b^{DL} are the vertical dark-to-light gradients of the image at pixels a and b respectively, w_{min} is the minimum weight of the graph.

For Bruch's membrane, a separate adjacency matrix is used with weights as:

$$w'_{ab} = \text{normalize}(-(g_a^{LD} + g_b^{LD}),2,4) + \text{normalize}(-(g_a^{DL} + g_b^{DL}),0,0.2) + \text{normalize}(-d_{ab},2,4) + w_{min} \quad (12)$$

where, g_a^{LD} and g_b^{LD} are the vertical light-to-dark gradients of the image at pixels a and b respectively, d_{ab} is the Euclidian distance from pixel a to b.

For the inner RPDEC boundary following equation is used:

$$w_{ab} = \text{normalize}(-(i_a + i_b),0,1) + w_{min} \quad (13)$$

The mean differences in the measured thicknesses of the total retina and RPEDC layers were 4.2 ± 2.8 and 3.2 ± 2.6 µm for automatic versus manual segmentation for 220 B-scans across 20 patients. The average segmentation time per image was 1.7 seconds automatically versus 3.5 minutes manually. The result for this paper is shown in Fig. 8.

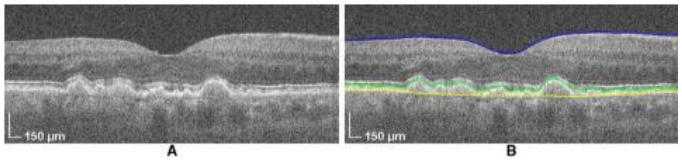

Fig. 8. SD-OCT images of eyes with intermediate AMD, without and with automatic segmentation. (A)A high-quality image with both large and small drusen, (B) the segmented image of (A) [10].

In the above two papers, the authors took the help of two certified graders for comparing their results, but the graders were not able to get perfect agreement between them whereas the automatic segmentation software was successful in achieving consistency in its segmentation results.

Vermeer et al. (2011) [11] uses manually segmented scans to learn from before automatically segmenting the layers for normal and glaucomatous eyes. As a classifier they used Support Vector Machine [21] which is used to learn and classify the pixels. Before training the classifier, the features are defined based on A-lines which give rise to a feature vector for each pixel. The classifier subsequently classifies and labels these feature vectors, which are regularized by using level set methods, which embed the interface implicitly and has some computational advantages (i.e., regarding propagation and topology of the interface). Finally, smooth interfaces are produced. Here 5 interfaces (between vitreous and RNFL, between RNFL and GCL/IPL, between IPL and INL, between OPL and ONL and between RPE and choroid) were evaluated for normal eyes and glaucomatic eyes. After comparing the auto- mated segmentation result, RMS error for the top and bottom of the retina were found between 4 and 6 µm and for inner retinal layers between 6 and 15 µm. The Fig. 9 and Fig. 10 shows the segmented result normal and glaucomatous eye respectively.

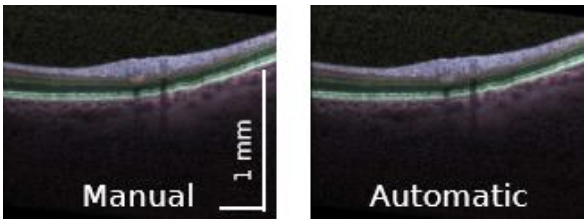

Fig. 9. Manually (left) and automatically (right) labeled B-scan of a normal eye [11].

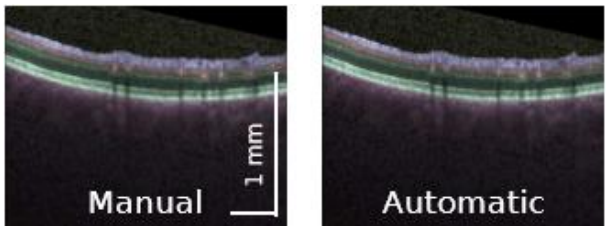

Fig. 10. Manually (left) and automatically (right) labeled B-scan of a glaucomatous eye [11].

Lang et al. (2013) [15] uses a Random Forest (RF) classifier [24] to segment 8 retinal layers. The classifier learns the boundary pixel and generates a probability map for each boundary which is further processed to finalize the boundary. The authors first performed intensity and spatial normalization followed by flattening the layers to Bruch's Membrane. They, then, found the top and bottom boundaries of the retina by computing image derivative of each A-scan using a Sobel kernel. The 27 features are calculated at each pixel which is used as inputs to the trained RF classifiers which produces boundary probabilities. The boundary refinement algorithm is applied on these probabilities and final retinal segmentation is obtained. They implemented and evaluated two methods to generate boundary curves from boundary probabilities. In the first method they used Canny Edge detection algorithm and in the second, they used optimal graph based search algorithm. Their result is shown in the Fig. 11.

Srinivasan et al.(2014) [12] proposes a method that automatically detects retinal disease which makes use of Histogram of Oriented Gradients (HOG) [26] descriptors and SVMs to classify image. This method successfully identified cases with DME and AMD without any human inputs. They denoised the image using a block matching and 3D filtering method [34] which is a image denoising strategy based on an enhanced sparse representation in transform domain. The enhancement of the sparsity is achieved by grouping similar 2D image fragments (e.g., blocks) into 3D data arrays which is

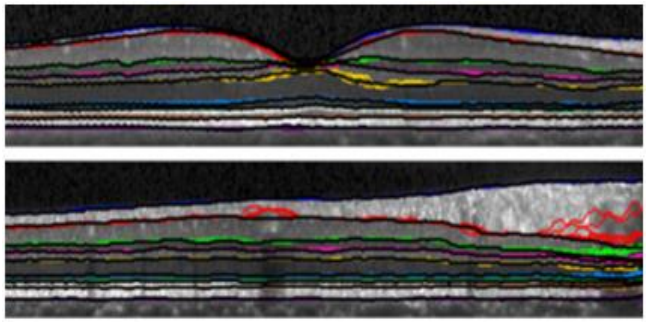

Fig. 11. Two B-scan images from two different subjects are shown with the resulting boundaries. Each boundary is represented by a different color with the manual delineation shown atop the other boundaries in black. Therefore, if the color is not visible at a particular point, the automatic and manual segmentation are in agreement [15].

calculated and fitted to a second order polynomial. Then the image is cropped and HOG descriptor algorithm is applied which divides the image into connected regions, called cells and a 1-D histogram of the directions of the spatial gradients, weighted by the gradient magnitudes, is calculated for each cell. These gradient values are then contrast-normalized over larger overlapping spatial blocks. Finally for classification SVM is used. As result, their classifier successfully classified cases of AMD, DME and normal subjects with 100%, 100% and 86.67% respectively. In this research work the authors emphasized on detecting AME and DME, rather than segmenting retinal layers.

Hussain et al.(2016) [14] proposes a method which identifies 4 retinal layer boundaries in presence of 3 pathologies-VMT, drusen and OCT defined atrophy. After denoising, they computed three approximate reference layers to identify ILM-RNFL boundary, the RBC boundary, ISL-EZ boundary and IZ-RPE boundary by using their relative position and pixel intensities. The position of the three pixels that represent the approximate locations of Retinal nerve Fiber layer(RNFL), Outer Nuclear Layer (ONL) and Retinal Pigment Epithelium (RPE) is given by C which is:

$$C_{RNFL,RPE,ONL} = \text{argmax}\,(I(RNFL) + I(RPE) - I(ONL)) \qquad (14)$$

where, I represents intensity.

They selected the edge pixels using Canny Edge detection algorithm and formed candidate pixels and defined the region of interest. Then, in the region, the candidate pixels are grouped and the start and the end points of each group are ascertained. After that, they calculated edge weights using the following equation:

$$\omega_{a,b} = \varphi_{a,b} + \psi^{r}_{a,b} + \gamma_{a,b} \qquad (15)$$

where, $\varphi_{a,b}$ represents the spatial distance between pixels a and b, $\psi^{r}_{a,b}$ represents slope between a and b relative to an already determined reference line (r) and $\gamma_{a,b}$ represents how well the pixel group containing b matches predefined properties of pixels forming the boundary, and applied Dijkstra's shortest path algorithm. They took into account pixel distance, slope similarity and non-associativity of the layers for edge weight calculation. Each time they identified a boundary they reduced the search region to increase the accuracy. The authors compared their result with 5 state-of-the-art methods: AURA tools, IOWA reference algorithm, Dufour's software, OCTRIMA-3D and Chiu et al. and it proved to be better than these methods. Fig. 12 shows its result.

There are also some medical papers which address different issues of infant eyes. These are basically case studies which concerns progression of a medical condition and the affects of it. Some papers deals with the impact of macular edema in infants with ROP and non-ROP [31]. It was observed that Visual Acuity was worst in the group with ROP+edema than infants without edema and ROP. Similarly, the birth weight was less and mean central foveal thickness was more in the former group. Some papers do emphasize the use of hand-held OCT systems for premature babies [33] and its advantages over the conventional OCT system and brings to light the persistence of Inner Retinal Layers in the foveal center and that the thickness of these layers gradually decreases with time to form the foveal pit, whereas, the Photoreceptor Layers tend to increase in thickness progressively [32]. The medical papers address the concern of childhood blindness and the attributes of ROP to the cause. This malice has hold its ground for the lack of proper detection procedure, but with the development of the

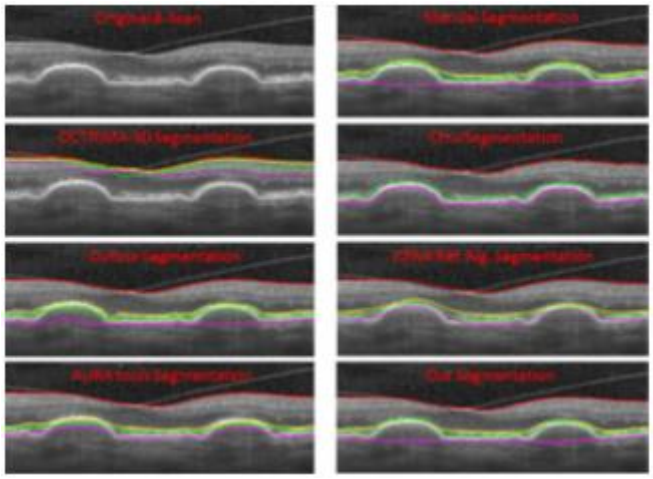

Fig. 12. Segmentation outputs by manual, OCTRIMA-3D, Chiu et al., Dufour et al., IOWA Reference Algorithm, AURA Tools and the proposed method. The ILM-RNFL, ISL-EZ, IZ-RPE, and RBC boundaries are de- lineated using red, yellow, green, and magenta lines, respectively [14].

techniques of monitoring the retinal layers of infants and the information deduced from the segmentation of the layers a ray of hope is seen for eradicating the affects of ROP. A brief description of ROP is given in the following sub-section.

A. Retinopathy of Prematurity(ROP)

Retinopathy of prematurity is an eye disease which affects infants born prematurely [35]. It is caused by abnormal and disorganized growth of blood vessels of the retina which may lead to scarring and retinal detachment. Different risk factors supporting the cause of ROP are:

- Prematurity
- High exposure to oxygen

- Low birth weight
- Various types of infections
- Cardiac defects

During development of the retinal blood vessels, they grow from the center part of the retina to outwards. This process is completed a few weeks before the normal time of delivery. However in premature babies it is incomplete and abnormal growth of the vessels take place. Normally the blood vessels grow in the relatively low oxygen concentrated areas of the retina and do not grow into the vitreous humor. In neonatal ICU, the premature babies come in contact with excess oxygen and normal blood vessels degrade and cease to develop. When this excess oxygen condition is removed, the blood vessels rapidly begin forming in an uncontrolled fashion and grow into the vitreous humor of the eye, which may lead to bleeding of the vessels inside the eye [36] [37]. When the blood and disorganized vessels are reabsorbed, it may give rise to a membranous structure which can pull the retina and lead to retinal detachment and eventually to blindness.

The severity of the disease is described in 5 stages [35]: **Stage 1 ROP**: It signifies development of a demarcation line between the normal retinal vessels developed retina and avascular retina, where vessels have not developed.

Stage 2 ROP: It signifies development of a demarcation ridge between the normal retinal vessels developed retina and avascular retina, where vessels have not developed. The demarcation line of stage 1 gains height and width and extends above the retinal surface.

Stage 3 ROP: It signifies neovascularization in the stage 2 demarcation line and leads to extraretinal proliferation of tissues. The new vessels grow into the vitreous gel in the middle of the eye, which incites fibrous proliferation. The ridge may now bleed and cause traction on the ridge.

Stage 4 ROP: It signifies that retinal detachment has started to occur due to the traction of the fibrous and the vascular tissue over the ridge. It is called 4A when the retinal detachment spares the macula and stage 4B when retinal detachment involves the macula.

Stage 5 ROP: It signifies total retinal detachment.

III. CONCLUSION

To sum up, this paper describes briefly some of the research works related to segmentation of retinal layers in retinal OCT images and also highlights the observations of some medical papers which address different issues related to retinal layers of infants, besides giving a brief idea about image segmentation, OCT and ROP. The researchers have been continually striving to develop automatic segmentation algorithm to segment the retinal layers in an OCT image, images of low resolution included and reduce the time of operation of the algorithm. The priority is accuracy and reproducibility of the results. However, a software that segments all the retinal layers of disease affected eye accurately is yet to be developed. Although there is a software named DOCTRAP, developed by Duke University, it is not commercially easily available in India. If all the layers of disease affected retina were segmented, it would be a significant step in understanding the behaviour of the layers and impact on the layers because of the pathology. Also proper and accurate information about thickness and other requisite data could be obtained from segmentation, which would go a long distance in assisting the doctors in proper diagnosis of a disease.

REFERENCES

[1] https://en.wikipedia.org/wiki/Image_segmentation

[2] http://en.wikipedia.org/wiki/Optical_coherence_tomography

[3] https://www.ncbi.nlm.nih.gov/pmc/articles/PMC3785070/?report=printable

[4] Committee for the classification of Retinopathy of Prematurity (Aug 1984).“An international classification of retinopathy of prematurity". Arch Opthalmol. 102 (8): 1130-1134. PMID 6547831 I.S. Jacobs and C.P. Bean, “Fine particles, thin films and exchange anisotropy,” in Magnetism, vol. III, G.T. Rado and H. Suhl, Eds. New York: Academic, 1963, pp. 271-350.

[5] Delia Cabrera Fernández, Harry M. Salinas, and Carmen A. Puliafito, “Automated detection of retinal layer structures on optical coherence tomography images," Opt. Express 13, 10200-10216 (2005) .

[6] F. Rossant, I. Ghorbel, I. Bloch, M. Paques and S. Tick, “Automated segmentation of retinal layers in OCT imaging and derived ophthalmic measures," 2009 IEEE International Symposium on Biomedical Imag- ing: From Nano to Macro, Boston, MA, 2009, pp. 1370-1373.

[7] Lee JY, Chiu SJ, Srinivasan PP, et al. Fully automatic software for retinal thickness in eyes with diabetic macular edema from images acquired by Cirrus and Spectralis systems. Invest Ophthalmol Vis Sci. 2013;54:7595-7602.

[8] J. Duan, C. Tench, I. Gottlob, F. Proudlock and L. Bai, “Optical coherence tomography image segmentation," 2015 IEEE International Conference on Image Processing (ICIP), Quebec City, QC, 2015, pp. 4278-4282.

[9] Z. Gao, W. Bu, X. Wu and Y. Zheng, “Intra-retinal layers segmentation of macular OCT images based on the graph optimal approach," 2016 9th International Congress on Image and Signal Processing, BioMedical Engineering and Informatics (CISP-BMEI), Datong, 2016, pp. 1359-1364.

[10] Stephanie J. Chiu, Xiao T. Li, Peter Nicholas, Cynthia A. Toth, Joseph A. Izatt, and Sina Farsiu, “Automatic segmentation of seven retinal layers in SDOCT images congruent with expert manual segmentation," Opt. Express 18, 19413-19428 (2010).

[11] K. A. Vermeer, J. van der Schoot, H. G. Lemij, and J. F. de Boer,“Automated segmentation by pixel classification of retinal layers in ophthalmic OCT images," Biomed. Opt. Express 2, 1743-1756 (2011).

[12] Pratul P. Srinivasan, Leo A. Kim, Priyatham S. Mettu, Scott W. Cousins, Grant M. Comer, Joseph A. Izatt, and Sina Farsiu, “Fully automated detection of diabetic macular edema and dry age-related macular degeneration from optical coherence tomography images," Biomed. Opt. Express5, 3568-3577 (2014).

[13] Stephanie J. Chiu, Joseph A. Izatt, Rachelle V. O’Connell, Katrina P. Winter, Cynthia A. Toth and Sina Farsiu, “Validated Automatic Segmentation of AMD Pathology Including Drusen and Geographic Atrophy in SD-OCT Images",Invest Ophthalmol Vis Sci. 2012;53:53- 61.

[14] M. A. Hussain et al., "Automatic Identification of Pathology-Distorted Retinal Layer Boundaries Using SD-OCT Imaging," in IEEE Transac- tions on Biomedical Engineering, vol. 64, no. 7, pp. 1638-1649, July 2017.
[15] Andrew Lang, Aaron Carass, Matthew Hauser, Elias S. Sotirchos, Peter A. Calabresi, Howard S. Ying, and Jerry L. Prince, "Retinal layer segmentation of macular OCT images using boundary classification," Biomed. Opt. Express 4, 1133-1152 (2013).
[16] M. Born; E. Wolf (2000). Principles of Optics: Electromagnetic theory of propagation, interference and diffraction of light. Cambridge University Press. ISBN 0-521-78449-2.
[17] Lavanya Chidambara, Chaitra Jayadev, Shwetha Mangalesh, Munusamy Sivakumar, Bhujang Shetty, Anand Vinekar,Eur J Ophthalmol 2015; 00 (00): 000-000.
[18] J. Weickert, B.M.T.H. Romeny and M.A. Viergever, "Efficient and Reliable Schemes for Nonlinear Diffusion Filtering," IEEE Trans. on Image Processing, Vol. 7, No. 3, pp. 398 - 410, 1998.
[19] C. Xu and J. L. Prince, "Snakes, Shapes, and Gradient Vector Flow," IEEE Trans. on Image Processing, Vol. 7, No. 3, pp. 359- 369, Mar. 1998.
[20] S. Geman and D. Geman, "Stochastic Relaxation, Gibbs Distribution, and the Bayesian Restauration of Images," IEEE Transactions on Pattern Analysis and Machine Intelligence, Vol. PAMI-6, No. 6, pp. 721-741, Nov. 1984.
[21] V. N. Vapnik, The Nature of Statistical Learning Theory (Springer- Verlag, 1995).
[22] J. Weickert, "Coherence Enhancing Diffusion Filtering" Int. J. Com- put. Vision 31, 111-127 (1999)
[23] G. Gilboa, N. Sochen and Y. Zeevi,"Image enhancement and denoising by complex diffusion process", IEEE Trans. PAMI 25 (8), 1020- 1036,(2004)
[24] L. Breiman, "Random forests," Mach. Learn. 45, 5-32 (2001).
[25] Leonid I Rudin, Stanley Osher, and Emad Fatemi, "Nonlinear total variation based noise removal algorithms," Physica D: Nonlinear Phenomena, vol. 60, no. 1, pp. 259-268, 1992.
[26] N. Dalal and B. Triggs, "Histograms of orientedgradients for human detection," in IEEE Computer Society Conference on Computer Vision and Pattern Recognition, 2005(IEEE, 2005), pp. 886-893.
[27] Pietro Perona and Jitendra Malik, "Scale-space and edge detection us- ing anisotropic diffusion," Pattern Analysis and Machine Intelligence, IEEE Transactions on, vol. 12, no. 7, pp. 629-639, 1990.
[28] E. W. Dijkstra, 'A note on two problems in connexion with graphs," Numerische Mathematik 1(1), 269-271 (1959).
[29] Joachim Weickert, Anisotropic diffusion in image processing, vol. 1, Teubner Stuttgart, 1998.
[30] M. A. Jayaram, Hasan Fleyeh, "Convex Hulls in Image Processing: A Scoping Review ",American Journal of Intelligent Systems 2016, 6(2): 48-58.
[31] Vinekar A, Mangalesh S, Jayadev C, Bauer N, Munusamy S, Kem- manu V, et al. Macular edema in Asian Indian premature infants with retinopathy of prematurity: Impact on visual acuity and refractive status after 1-year. Indian J Ophthalmol 2015;63:432-7.
[32] Anand Vinekar, Shwetha Mangalesh, Chaitra Jayadev, Ramiro S. Maldonado, Noel Bauer and Cynthia A. Toth, Review Article Retinal Imaging of Infants on Spectral Domain Optical Coherence Tomogra- phy, Hindawi Publishing Corporation BioMed Research International Volume 2015, Article ID 782420, 12 pages.
[33] Mallipatna A, Vinekar A, Jayadev C, Dabir S, Sivakumar M, Krishnan N, et al. The use of handheld spectral domain optical coherence tomography in pediatric ophthalmology practice: Our experience of 975 infants and children. Indian J Ophthalmol 2015;63: 33586-93.
[34] K. Dabov, A. Foi, V. Katkovnik and K. Egiazarian, "Image Denoising by Sparse 3-D Transform-Domain Collaborative Filtering," in IEEE Transactions on Image Processing, vol. 16, no. 8, pp. 2080-2095, Aug. 2007
[35] http://en.wikipedia.org/wiki/Retinopathy_of_prematuri ty
[36] Kumar, Vinay (2007). "Chapter 29: Eye, Retina and Vitreous, Retinal Vascular Disease." Robins basic pathology (8th ed.). Philadelphia: Saunders/Elsevier. ISBN 978-1416029731
[37] Guyton, Arthur; Hall, John (2006). "Chapter 17: Local and Humoral Control of Bloood Flow by the Tissues". In Gruliow, Rebecca. Textbook of Medical Physiology (Book) (11th ed.). Philadelphia, Pennsylvania: Elsevier Inc. p. 200. ISBN 0-7216-0240-1.

S.R. Nirmala received the B.E. degree in Electronics and Communication Engineering from Jagadguru Murugarajendra Institute of Technology, Chitradurga, India, in 1990. She obtained the M.Tech. degree in industrial Electronics from the National Institute of Technology Karnataka (NITK), Surathkal, India, in 1997; and the PhD degree in Electronics and Communication engineering from the Indian Institute of Technology (IIT) Guwahati , Assam,India, in 2012. She is currently working as Assistant professor in the Department of E.C.E., Gauhati University Institute of Science and Technology.

H Pallab Jyoti Dutta completed his B.E. in Electronics and Telecommunication Engineering from Jorhat Institute of Science and Technology, Jorhat, Assam in 2016 and currently pursuing M. Tech in Signal Processing and Communication in Gauhati University.

TABLE I: Segmentation work of different researchers.

YEAR	RESEARCH WORK	RESULT	METHODS USED
2005	Fernandez et al.	7 edges are extracted for normal eyes but for eyes with pathology, the method is not satisfactory.	Non-linear complex diffusion process, Coherence enhanced diffusion process, Automatic peak finding procedure, Linear interpolation.
2009	Rossant et al.	8 layers detected & thickness result compared with 5 experts.	Active contours, K-means, Markov random fields, Kalman filter.
2010	Chiu et al.	7 layers of normal eyes detected. Compared the result with 2 experts for thickness of layers.	Graph theory and dynamic programming.
2011	Vermeer et al.	5 interfaces for normal & glaucomatic eyes & thickness maps were derived.	Feature extraction, Classification (SVM), Regularization.
2012	Chiu et al.	3 retinal boundaries of eyes with drusen and geographic atrophy. Compared the result with 2 expert graders.	Graph theory and dynamic programming.
2013	Lee et al.	3 layers detected. Compared DOCTRAP results with Spectralis & Cirrus.	Graph theory and dynamic programming.
2013	Lang et al.	9 retinal layer boundaries are detected.	Random forest classifier, Boundary refinement algorithm.
2014	Srinivasan et al.	Detected DME & AMD cases accurately. Emphasized on detection of diseases rather than segmenting retinal layers.	HOG descriptors, SVM.
2015	Duan et al.	7 layers detected for normal eyes.	Variational retinex model, Non-linear diffusion processes, Unsharp masking.
2016	Hussain et al.	Detected 4 retinal layers with pathologies & compared the result with 5 state-of-the-art techniques.	3 approximate reference layers computed, Graph cut, Shortest path algorithm.
2016	Gao et al.	Segmented 10 retinal layers.	Graph optimal approach, canny edge detector

TABLE II: Performance Measure

AUTHORS	IMAGES CONSIDERED	PERFORMANCE
Fernandez et al.	72 OCT scans from normal subjects.	Thickness of segmented layers was mapped.
Rossant et al.	72 images from 25 normal subjects.	A distance between the manually traced curves and the ones obtained by the proposed method was calculated. The distance varies from 1.8 pixels for the RNFL/GCL+IPL interface, to 4 pixels for the OPL/ONL.
Chiu et al. (2010)	Volumetric scans acquired from 10 normal adults.	Mean difference in total retinal thickness between two expert manual graders as compared to the thickness differences between the automatic segmentation and an expert is 2.22 pixels and 0.92 pixels respectively.
Chiu et al. (2012)	Total of 220 B scans from 20 volumes.	The mean differences in the measured thicknesses of the total retina and RPEDC layers were 4.2 ± 2.8 and 3.2 ± 2.6 μm for automatic versus manual segmentation.
Vermeer et al.	10 healthy and 8 glaucomatous subjects.	RMS errors for the top and bottom of the retina were between 4 and 6 μm, while the errors for intra-retinal interfaces were between 6 and 15 μm.
Lee et al.	40 SDOCT scans from 20 subjects for each Spectralis and Cirrus systems.	The mean thickness in the 1-mm central area determined by DOCTRAP and Spectralis was 463.8 ± 107.5 μm and 467.0 ± 108.1 μm, respectively and the mean thickness in the 1-mm central area was 440.8 ± 183.4 μm and 442.7 ± 182.4 μm by DOCTRAP and Cirrus, respectively.
Lang et al.	Data from right eye of 35 subjects-21 diagnosed with Multiple Sclerosis and 14 normal.	9 retinal layers delineated to an accuracy of at least 4.3 microns for any of these 9 boundaries.
Srinivasan et al.	Dataset of 45 OCT volumes with 15 normal, 15 with AMD and 15 with DME.	Classified cases of AMD, DME and normal subjects with 100%, 100% and 86.67% respectively.
Hussain et al.	Three datasets- Chiu et. al., Tian et. al. and from Center for Eye Research Australia	The mean and standard deviation of the root-mean-square error in the form of mean ± standard deviation in pixels for proposed method is 1.57 ±0.69, which is lower than compared to the existing top five methods with 16.17±22.64, 6.66±9.11, 5.70±10.54, 3.69± 2.04, and 2.29±1.54.
Gao et al.	Two datasets containing 51 and 13 slices	The unsigned border positioning errors between the proposed algorithm and the reference standard were approximated to 1 pixel and the signed border positioning errors were approximated to -0.03 and 0.16 pixels and were smaller than those computed between two observers.